Anomalous Behaviour for Microhardness of Al-3wt.% Mg alloy

F. Abd El-Salam[a], R.H.Nada[a], H. Abd El Aziz[b], E. Abd El-Rheim[b]

a) Department of Physics, Faculty of Education, Ain Shams University, Cairo, Egypt.
b)Tabbin Institute for Metallurgical Studies (TMS), Helwan
E-mail: drfadad@hotmail.com

Microhardness measurements, H, were obtained for sheets of Al-3wt.% Mg alloy in the temperature range 443-503 K, applied loads 10-300 gm and dwell times 10-40 sec. The age-hardening curves showed off leveling and pronounced oscillations indicating instability reflecting a competition between the effect of dynamic recovery or sub-structures coarsening and the effect of solute drag and precipitation hardening. The indentation size effect index (ISE), m, was calculated as 2 for the binary alloy indicating that, H, is independent on indentation size. Increasing temperature, T, load, L, and dwell time, t, caused a decrease in, H, due to the decrease of the amount of free Mg available for further precipitation hardening during the aging process. In general, increasing temperature, dwell time, applied load caused a decrease in hardness.

1. Introduction:

Weight reduction, reducing fuel consumption and improving fuel efficient become a key focus area because of the demand for light-weight alloys for structural applications [1,2**].** In this respect, Aluminum (Al) alloys of which the alloys 5XXX with Magnesium (Mg) as the major alloying element have been considered for use in a wide variety of applications[1]. . As wrought non-heat treatable alloys, their strength is derived mainly from solid solution strengthening by Mg which has a substantial solid solubility in Al, and strain hardening [3].

The decomposition of the supersaturated Al-Mg solid solution by aging can be presented as follows: formation of GP zones immediately within seconds from the quench [4b], in high energy areas (grain boundaries and

dislocations) but they are small and most of the excess vacancies remain around them as a cloud with a little or no contribution to hardening. The critical temperature upon which zones do not form is very low 320-340 K [4b]. Above this temperature aging starts with the formation of the coherent and hexagonal β`-phase, which forms first at the grain boundaries and produces a solute depleted zone around them, and another vacancy depleted zone in which little or no precipitation occurs even after β` has precipitated in the centre of the grain [4b] at 398-498 K. The FCC stable β-phase is formed above 523K. β-phase is usually given as Mg_2Al_3 [4b] where as the formula Mg_5Al_8 fits the composition and most the structures given. At (523-693K) β` and β phases dissolve [4b]. On aging the supersaturated Al-Mg alloy a featureless fine structure was observed prior to the thermally induced GP zones which form by a growing process for the amount of the GP zones formed within seconds from the quench [4b]. On the other hand, it was reported [5] that in the beginning of heating a partial annealing out of the quenched defects takes place. β`- phase precipitates are believed to form above 400K. Above 450K, phase precipitates begin to dissolve and above 550K the stable β-phase is believed to form directly from the matrix, with loss of coherency, which is in agreement with the formation of the stable β (Mg_5Al_8) precipitates in Al matrix reported previously [4b]. Hardness as a complex property related to the strength of interatomic forces, is defind as the resistance of a material to local plastic deformation. Microhardness testing can be the easiest way to determine the mechanical properties of the different phases of the structure and follow aging behaviour during phase decomposition sequence [6] even at high temperature [7]. Hardness measurement can be related to mechanical properties such as yield stress σ_y, where in bulk materials [8]: $H=3\sigma_y$ .....(1)

A functional relationship between hardness H and temperature (T) has been reported as [9], $H= H_O \exp(-\alpha T)$ ……. (2)

where H_O is the hardness at zero K, or the intrinsic hardness, and α is the softening coefficient [7] or the coefficient of thermal expansion [10]. The Vickers microhardness, H, is defined as [11],

$$H_v= 1.8544 (L / \ell^2) \quad \text{…….....} \quad (3)$$

where L is the applied load and ℓ is the indentation size. The maintained indenter at a constant load, over a period of time and under well controlled conditions penetrates and causes the material beneath the indenter to creep.
The changes in the indentation size are therefore monitored [7]. It was reported [10] that hardness decreases with indentation time, following a function of the form [11], $H=H_1 t^{-k}$ …… (4)

where H_1 is the hardness at a given reference time t =1 and k is the so-called creep constant. Indentation- induced cracking phenomena and the apparent change in hardness value with change in indentation size, namely, the indentation size effect (ISE) [12] are intractable problems for Vickers hardness. In the discussion of the standard Vickers hardness test, the empirical expression, Meyer's law [13] relating the applied load L and impression diagonal ℓ, having the form: $L= K \ell^m$ ……(5).

where m is the Meyer exponent or (ISE) and K is the pre-factor, yields a constant value for the Meyer index, or the ISE index, m, of 2. Thus, hardness should be independent of indentation size. At low loads m does not equal 2 for Vickers indentation. More generally there is an increase in microhardness at small loads for most metals and alloys, namely, m‹2, showing that microhardness has a load dependent behaviour, i.e., ISE behaviour. A decrease in microhardness of as-cast Mg-5wt.% Al alloy with Ca addition was observed on increasing the applied load showing m value of 1.91, i.e., m‹ 2, which indicates that the traditional Meyer's law is suitable for describing the ISE behaviour of the tested alloy and the value of m suggests the presence of a weak ISE

2. Experimental procedure:

Aluminum-Magnesium alloy containing 3wt.% Mg was prepared from elements of 99.9% purity (Al), 99.9 (Mg). The alloy was prepared by weighting the proper ratios of the components and the composition was melt in graphite crucible placed in the stable zone of a muffle furnace adjusted at 1123K, which is a temperature above the melting point of Al and Mg. When Al is completely melt cleaner material is added to remove all the gases and the impurities inside it, then Mg is added to Al until it completely melt, and the casting was carried out in hot iron mould. The melt was cooled in iced water. The chemical composition of the binary Al-Mg alloy is shown in table 1.

Table 1:

Run	Si-L	Mg	Cu-L	Zn-L	Fe-L	Mn	Ti	Ni-L	Pb	Al%
Avg	0.11	3.091	0.038	0.102	0.14	0.15	0.01	0.005	0.007	96.4

All specimens were given an initial annealing for 8h, at 773K and then quenched in cold water. The ingot was rolled with intermediate annealing at 773K to obtain sheets of 7cm length, 3cm width and 0.1cm thickness. The microhardness measurements were obtained by using a Vickers indentor at load (L). The tested sheets were heated for 2h in the working temperature range from 443K to 503K in steps of 10K, then quenched in cold water kept at

room temperature (RT). The surface of any tested sample was polished by using polishing machine then examined by an optical microscope having magnification of 20X and 50X. Hardness indentation was obtained by applying automatically the loads (10, 50, 100, 300 gm) for the dwell times (10, 20, 30 and 40 sec). The two lines which move at opposite sides of the indentation, were adjusted to the edges of the indentation diagonals and the end button was pressed to show the mean diagonal value and the corresponding hardness value. To obtain the optical Micrographs, the specimen was heated at the selected temperatures (323, 373, 443, 473 K) for 2 h, quenched in cold water, then polished and etched by Keller's enchant (Distilled water 20 ml, HCl 32% 20 ml, Nitric acid 65% 20 ml, Hydrofluoric acid 40% 5ml) for 5 s, and then the surface morphology was studied by optical microscope at 20x, 50x magnification.

3. Experimental results:

The effect of aging temperature (T), dwell time (t), applied load (L), on the Vickers micro hardness values H for the binary Al-3wt.%Mg alloy is given in Fig.1. Fig. 1(a-d) shows the temperature dependence of H under the applied loads 10, 50, 100 and 300 gm and the dwell times: 10s, Fig. (1a); 20s, Fig. (1b); 30s; Fig. (1c) and 40s, Fig. (1d). The absence of stable monotonic behaviour, the irregular thermally induced oscillations and the wavy form of the H-T curves indicate clearly that, these observations are due to the role of Mg atoms and the combined effect of all the factors T, t and L on H which reflects mainly the instable nature of the internal structure existing at certain temperature. The different initial H values show clearly the effect of the applied load L, Fig. (1a). H increases for the loads 10, 50, 100 gm at 453K while decreases for 300 gm load. At 463K H decreases for the loads 10 and 300gm while an increase is still observed for the loads 50 and 100gm. The behaviour is reversed at 473K for both 10, 300 and 50, 100 after which a general fall of H takes place with different values for all loads at 483K. This state of common decrease at 483K may point to a softening behaviour followed by an increase for all loads at 493K and 503K.. This indicates that these results are due to similar structures but of different levels depending on the applied load. Hardness increase reaches relatively high value for 300gm load. Increasing (t) to 20s, the magnitude of H variations for the load 300gm increased markedly showing high temperature dependence compared to those for the other loads, Fig. (1b). At 443K, H for 300gm, t =20s, increased to nearly twice the value for t=10s, then dropped to a minimum value 65 MPa at 463K. At 483K while it increased to 165 MPa, all the values of H for the other loads decreased than those at 473K. At 493K H dropped to 105 MPa for 300gm load, while values of H for the other loads slightly increased over those at 483K.

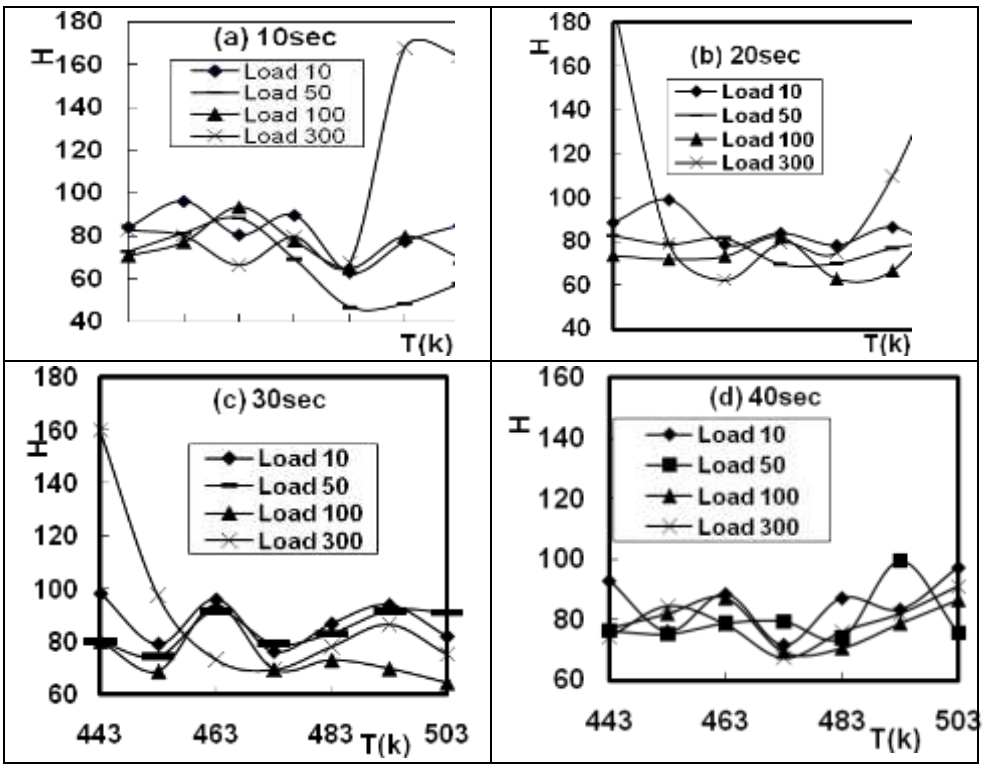

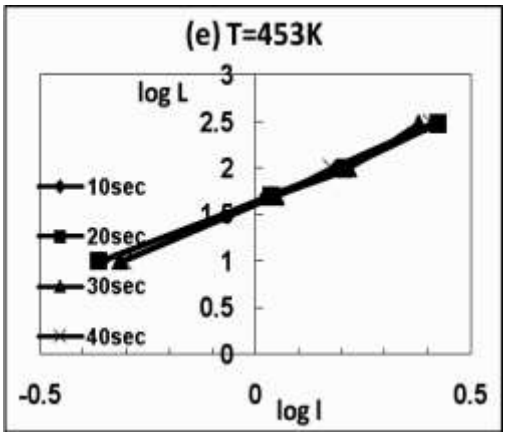

Fig.1:(a-d) Temperature dependence of the binary alloy hardness, H, under different loads and dwell times, (e) Relation between log Load, log L and log indentation diagonal, log l, for binary alloy under different loads at 453K, (f) Prefactor, k, in Meyer's law for different loads at 453K.

At 503K, H for 300gm increased to a high value of 170 MPa showing a decreased sequence for H values for all loads inconsistent with the behaviour known for decreasing H on increasing the applied load. For t =30s, a common decrease in H is observed at different temperatures but H for 300gm was still markedly high. For t=40s, a common decrease for H is still observed and the effect of temperature on H is more pronounced. It is observed that the variation of H may be the resultant of the effect of the applied load and dwell time at different temperatures, Fig. 1(a-d). According to Meyer's law (4), the study of the indentation size effect (ISE), indentation loads from 10 to 300gm were applied for the binary Al-3wt.% Mg alloy Fig. (1e), is a double logarithmic representation for the applied load, L and the corresponding indentation diagonal ℓ for the binary alloy. In Fig. (1e), the gradient of any curve, log L/log ℓ, is Meyer index, m, or ISE index. m values for the binary alloy and the pre-factor K in Meyer's law are given in Fig. (1f). The value of m for the binary alloy is calculated as 2.

Applying equation (1) to the data in Fig. (1a), the relation between ℓn H and T for the tested alloy under 10 gm load and 10s dwell time, as representative example, is plotted as shown in Fig. (2a). From the straight lines of Fig. (2-a), the value of the softening coefficient α is obtained as the slope and the intrinsic hardness at zero Kelvin, H_o, is obtained from the intercept at ℓn H axis. The obtained values of α and H_o are plotted against time t as given in Fig. 2b. For the different temperatures, the oscillations still occur and the order of hardness values at 503K differs from that at 443K. Fig. (2c) shows the time dependence of H under different loads at 453K. The effect of dwell time, t, is clear as the hardness decreases markedly with increasing dwell time. According to equation (3), for the data of Fig. (2c), a plot relating ℓog H and ℓog t obtained under different loads at 453K, is given in Fig. (2d). From the slope, the creep constant k is calculated and its negative inverse gives the stress exponent n. From the intercept with ℓog H axis, the value of H_1, which is the hardness at reference time equals one second is obtained. The time dependence of k, n and H_1 is given in Fig.(3).

Also, applying equation (1), the temperature dependence of yield stress σ_y for the binary alloy under different loads and dwell times, is given in Fig. (4a-d). Optical micrographs with 50X for the binary alloy samples are given in Fig. (5).

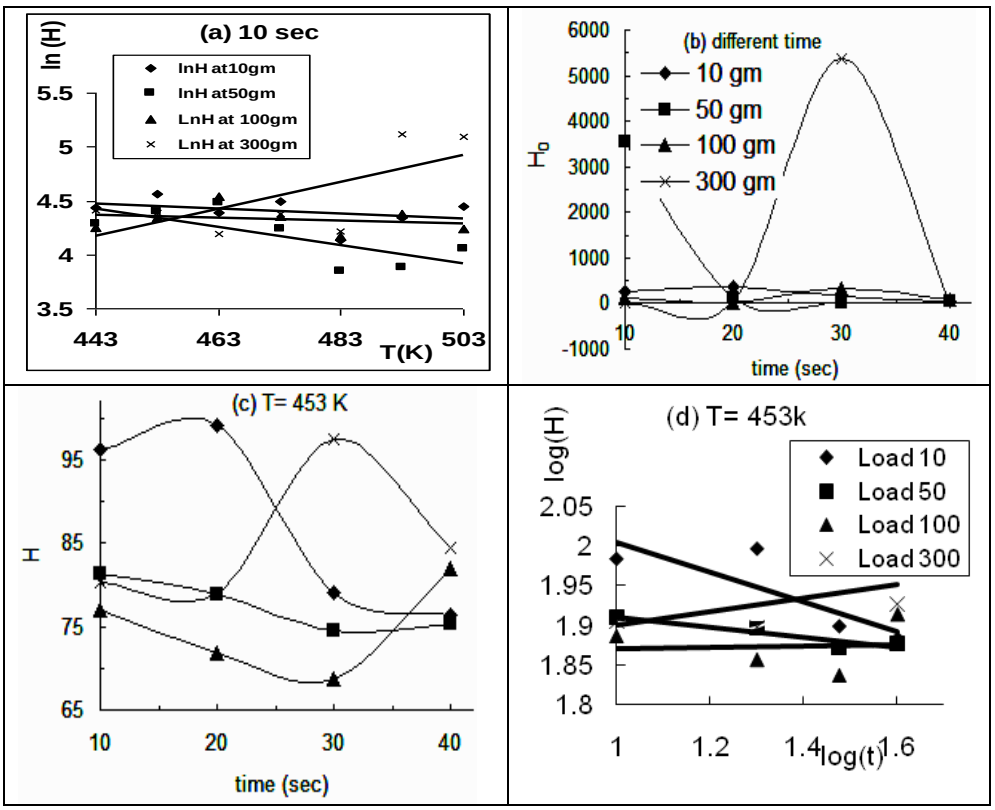

Fig.(2): Temperature dependence of: a) ln H, for the binary alloy sample under different loads at10 sec, (b) Values of α and H_o, **(c)** Hardness H at different loads and times, (d) log H and log t under different loads at 453K

4. Discussion

The stress fields around solute atoms interact with the stress field of a moving dislocation, thereby increasing the stress required for plastic deformation. The solute strengthening effect depends mainly on:

(i) The size difference between the solute and the solvent atoms. The more is the size difference, the more intense is the stress field around the solute atom and its interaction with the moving dislocation is correspondingly stronger. (ii) With a large concentration of the solute atoms, the moving dislocation interacts with the solute stress fields at many points along its length. In Fig. (1a), the initial hardness at 443K for the different loads, except for the load 300gm, decreased with increasing load from 10 to 100gm, which may be due to the increased dislocation activity [7] at this temperature, 443K, where the GP zones formed by quenching dissolve. Eliminating the indentation

diagonal ℓ, which varies [13] with load L according to equation (5), equation (3) becomes:

$$dH / dL = ((m-2)/m)\, k_1\, (k/L)^{2/m} \quad \text{…….....……..} \quad (6)$$

where k from equation (3) equals (1.8544).

A drop in hardness with increasing indenter load is therefore predicted because (m-2) is negative. This consists with hardness drop for higher loads in Fig.(1a). However, theoretical analysis of softening for smaller indentation was rendered to vibration [13] which becomes increasingly important as the load is reduced. More generally, the increased microhardness at lower loads for most metals and alloys where, ISE or the modulus m‹2 [13]. The unexpected increased hardness at the load 300gm at 443K, which is nearly of magnitude as that for the 10gm load, may be due to the effect of the increased stress generated by the applied 300gm load which decreases the size of the existing grains due to the formation of subgrains leading to a large number of small grains that cause increased hardness [14]. This increased hardness may be also due to: i) The formation of dislocation loops of vacancy type from the retained quenched-in defects and the high induced dislocation density. ii) The dissolution of the formed GP zones and the subsequent formation of β`-phase precipitates which are believed to form above 400K [5]. As β` formation progresses from the grain boundary to the centre, hardness increases and at temperatures above 523K re-crystallization of the matrix follows [4b]. The general observed increased hardness above 483K in Fig.1a may be due to the existence of the stable β-phase (Mg_5Al_8), which is known to be very brittle below 600K but shows some plasticity at higher temperatures, formed from β` at temperatures up to approximately 500K [4b]. The hardening effect of β-phase may be modified by the lower interfacial energy between Al and Mg_5Al_8 which allows rapid coagulation of precipitate particles [4b]. This takes place at tested temperatures below crystallization temperature, 523K, at which softening is expected to take place. The precipitate formed during the quench which has the equilibrium structure, β-phase, does not act as nucleus for precipitation during the aging, and the β-phase formed from the matrix is incoherent with the matrix [4b]. Therefore, the enhancement of β precipitates coagulation under some conditions can cause softening as clear from hardness drop above 493K under different dwell times such as that for load 100gm, (10, 20 s) Fig. 1(a and b); (10, 100, 300 gm), 30s Fig. 1c and 50gm, 40s Fig. 1d. This points to some role played by dwell time in indentation process which is in agreement with equation, (4). The leveling off and pronounced oscillations of the age-hardening curves in Fig. (1a), which were observed previously [15], were found in these curves beyond 443K provide a clear indication of instability. The hardness peaks observed for all the curves may correspond to different aging processes. These oscillations are readily understood in terms of

competition between a metallurgical reaction concerning the structure variations [15], besides the very effective role of Mg in reducing the rate of creep [4b], which tend to increase the hardness and the thermally induced intrinsic decrease in hardness with increasing aging temperature. The hardness therefore never produces the behaviour of homogeneity and stabilization as long as the reaction proceeds to completion until competition comes to an end and then a certain regular behaviour dominates, which is not attained in the curves obtained in the tested temperature range under the applied loads and the dwell times considered. This unstable behaviour cannot be explained here by the onset of re-crystallization, which occurs at a temperature higher than 523K [4b]. As can be seen from the optical micrographs of the as cast binary alloy given in Fig. 5(a-c), the alloy exhibit a typical dendritic structure. When increasing temperature, the dendritic structures become more obvious, and the dendrites are gradually refined. Moreover, some rod-like phase accumulates with cluster morphology in the alloy and some white particles can also be found. The cumulate rod-like phase decreases but number density of white particles increases. In the alloy the rod-like phase has changed to dissociative morphology, and a semi-continuous phase can be found, which is of lower strength than the rod-like phase.

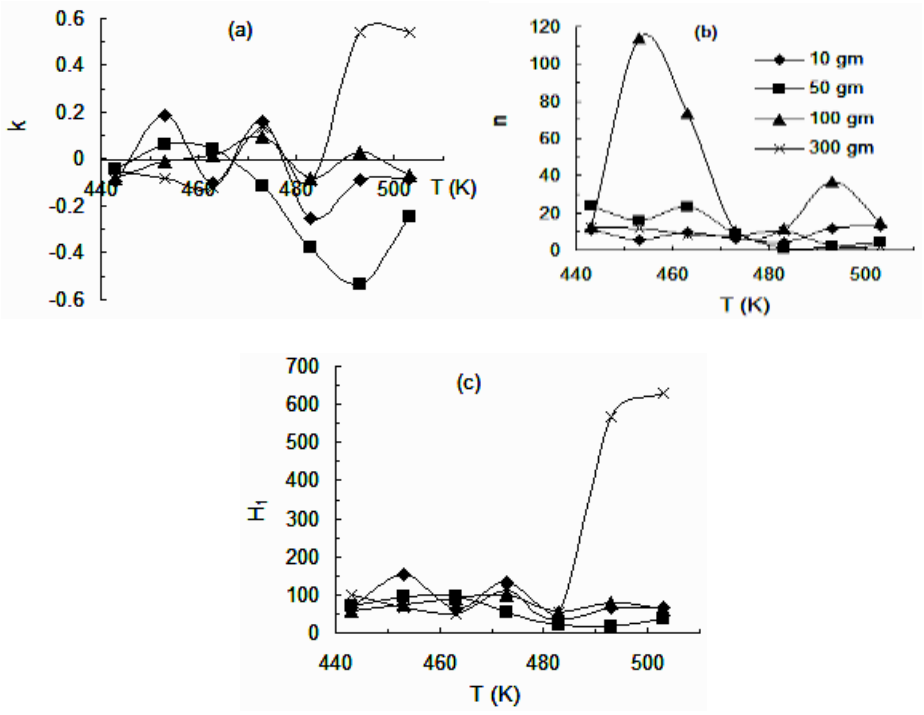

Fig.3: (a) creep rate, k, (b) stress exponent, n and (c) Time dependence of, H_1, Hardness at 1 sec

Diffusion of Mg is affected by other elements present: Cu, Si, and Zn reduce it, and Fe, Mn and Ni have little effect [4b]. It was proposed [15] that the observed oscillations in hardness curves of Figs. 1and 4 can be explained by the retention of iron, which is an impurity element of 0.143 wt.% in the present tested Al-Mg alloy, in the supersaturated solid solution after casting and wire drawing, and then its subsequent precipitation during aging. This indicates that the amount of iron removed from solution is less than the maximum solubility of 0.05 wt.% Fe near the melting point of Al [4a]. This explanation was supported by TEM micrograph which revealed the presence of newly precipitated iron in the tested commercial Al-Mg alloy, AA5005, samples after aging. This finding is consistent with the proposed explanation for a role of iron beyond 443K in the tested Al-3wt.% Mg alloy. It was found [16] that during the re-softening of quenched high purity Al a rapid decrease in loop density takes place in the temperature range (373-453K) while annealing above 453K, the kinked dislocations which form on the expense of loops are stabilized by impurity segregation causing a delay in the final re-softening. The Mg atoms when thermally activated would diffuse away rapidly along the high diffusivity path through the boundaries which become saturated causing the dislocation sources near the boundaries to be strongly pinned. High thermal activation and/or stress is therefore needed for yield, which is clear from the instability of the values of H, in Fig. (1), and σ_y, in Fig. (4). The decrease in H and σ_y is the result of the decrease in loop density. The vacancies emitted by the dissolving loops give rise to enhanced diffusion of Mg atoms toward the remaining loops and decorating them leading to an appreciable strength of the loops when the dislocation movement during plastic deformation takes place by cutting mechanism. The applied stress, σ, which is necessary to operate the cutting mechanism is given by the equation, [17].

$$\sigma\, b\, N^{-1/2} \,.\, 2a = \gamma\, \pi\, a^2 \qquad \ldots\ldots (7)$$

$$\text{or,} \quad \sigma = a\, \gamma\, (N\, \pi\, a^2)^{1/2} = a\, \gamma\, f^{1/2} \qquad \ldots\ldots (8)$$

where N is the dislocation loops per unit area with diameter a, γ is the energy necessary to cut through unit area of loop, b is the Burgers vector of the moving dislocation, f is the volume fraction of the loops. The condition for the existence of an extremum is:

$$f^{1/2}\, d\gamma/dT + \gamma\, df^{1/2}/dT = 0 \qquad \ldots\ldots (9)$$

The decrease of the number of loops gives rise to $df^{1/2}/dT < 0$, while because of the increasing number of the bound Mg atoms to loops $d\gamma/dT > 0$. Therefore, equation, 8, must have real solution for a minimum.

The increasing strength of the remaining loops after reaching the minimum will dominate until the yield stress reaches a maximum after which the dissolution of loops becomes the effective factor again, which is the case for the oscillations of the unstable curves of Figs. (1 and 4). At some higher temperature, e.g. above 483K, anneal hardening [17] process may take place as detected from the increase of H and σ_y in Figs. (1 and 4), respectively. This is probably a result of the formation and stabilization of kinked dislocations by Mg atoms. Accordingly, under the different conditions: aging temperature T, dwell time t and the applied load L, the hardness curves of Fig. (1a-d) show a general behaviour alternating between hardening and softening dominates all over the obtained data. This reflects the competition between the effect of dynamic recovery or sub-structures coarsening and the effect of solute drag and precipitation hardening which takes place during plastic flow of these materials [18]. Therefore, the dominant behaviour depends mainly on the structure existing at different temperatures and the testing conditions.

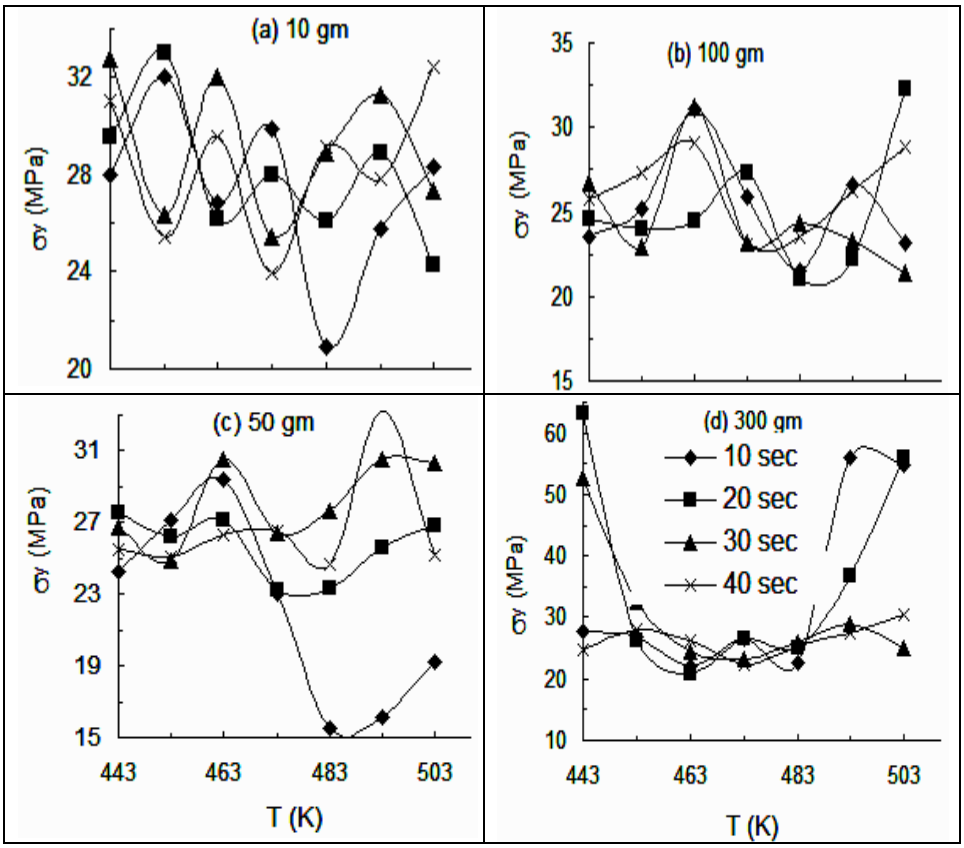

Fig.(4): (a-d) Temperature dependence of yield stress, σ_y , for the binary alloy as deduced from hardness data under different loads and dwell times.

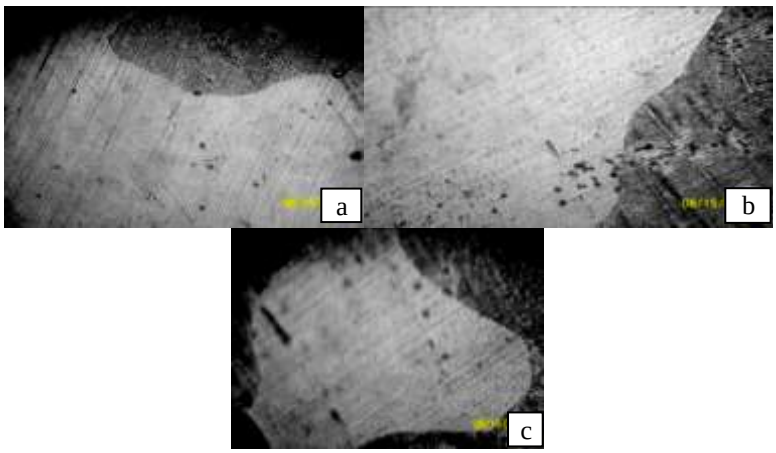

Fig.(5): Optical micrographs with 50X for Al-3wt.%Mg alloy.

The presence of high solute content in the matrix and the low deformation temperature may suppress the dynamic recovery contributing to the enhancement in hardness and strength [19]. The possible mechanism could be a grain refinement and strain hardening, which occur due to the higher dislocation density in the tested samples [20]. This consists with the initial increased hardness of the loads 10, 50 and 100 gm at 453K in Fig. (1a), while the reverse behaviour, i.e., decrease in hardness is observed with the 300gm load. At 453K the observed increased hardness in Fig. (1a-d) at certain dwell times may be due to the existence of precipitates having coherent strain field caused by the partially coherent interface with the matrix in the early stage of aging [21]. The intermediate β` particles, $Al_3Mg_2$, which nucleate on the quenched-in defects, form at temperatures above 400K [5], cause the main source of hardening in Al-Mg alloys. Moreover, the insufficient quenched-in defects which allow the nucleation of β`- phase leads to direct formation of the stable β-phase (Mg_5Al_8) from the matrix with loss of coherency [4b], which is associated with softening. In the tested temperature range, (443-503 K), it may be considered that the existing amount of the intermediate β`- phase leads to a corresponding level of hardness in the tested samples. On the other hand, the amount dissolved of β`- phase and/or the transition of the precipitates from coherent to incoherent with Al matrix lead to a decrease in hardness. The hardness minima at 483K in Fig. (1a) can be explained in terms of the formation of the incoherent stable β- phase. At higher dwell times, Figs. (1 and 4), it is clear that the amplitude and position of the irregular oscillations varied markedly as a result of the combined effect of the applied factors: T, t and L. Plastic instabilities of the strain rate softening type has been first explained on the basis of bulk diffusion with the collected repeated breakaway and recapture

of dislocations from their solute clouds of foreign atoms. In the developed approaches to unstable plastic flow, the novel concept is based on the realization that the ensemble of crystal lattice defects is a non-linear dynamical system characterized by self-organization phenomena [22].

Portevin-Le Chatelier (PLC) effect is a prototype of plastic instabilities in the context of physical nonlinear systems developing spatio-temporal patterns [23]. The complex spatio-temporal patterns observed include generation and propagation of localized deformation bands and concometent discontinuities of the deformation curves as those shown in Figs. 1 and 4 [24]. During plastic flow, the spatial arrangement of dislocation ensembles derives from interaction of dislocations with: i) strong and dense local obstacles like solute atoms where PLC effect takes place due to dynamic strain aging (DSA), i.e. a dynamic interaction between solute atoms which diffuse to mobile dislocations during their temporary arrest at local obstacles. ii) dislocations mutual interactions, which leads to the emergence of PLC effect as unstable plastic flow with regular or propagating patterns on the surface of the deformed material, or plastic instabilities in stress strain curves [25].

Jerky flow or the PLC effect is one of the most prominent examples of such observed plastic instabilities [25]. 5XXX (Al-Mg) alloys are the prototype for observing the PLC effect with its variances [26]. Deformed 5XXX (Al-Mg) alloys are characterized by a relatively uniform distribution of dislocations. This is because of the solute drag effect which prevents dislocations from undergoing further rearrangement to lower energy structures [27]. In Al-Mg systems the effect of Mg atoms on the work hardening behaviour of low solute alloys is more sensitive to the temperature changes than that of highly alloyed systems. This points again to the concept of competition which takes place during plastic flow [18]. When the number of solute atoms reaches such a value as to be enough to surround the moving dislocation, the hardness reaches maximum value as the case of the observed maxima in the curves of Figs. (1and 4). The increase of temperature makes the dislocation overcome the obstacle leading to the observed minima in Figs. (1 and 4), depending on the state of the tested sample under the applied conditions. The ISE index, m, calculated as 2 for the binary Al-3wt.% Mg shows that its measured hardness, H, should be independent on indentation size. (As shown in Fig. 1f) the pre-factor K in Meyer's law increases with increasing the applied load for the binary alloy. It is well known [1] that Mg has a higher affinity for elements such as Sn, Si or Pb than for Al, and can form binary intermediate compounds with Al only after these elements are completely combined..

During quenching from the solution heat treatment temperature, the Mg cool more slowly than the α-Al phase. This causes the α-Al phase around the hard inter-metallic phase of Mg to be warmer than the bulk α-Al phase [28]. The high dislocation density and the high solubility centres (the warm inter-metallic phase- α-Al phase interfaces) in the alloy are favorable conditions for precipitation formation. This increases the volume fraction of precipitates in age hardened alloy. The observed decrease of hardness with dwell time, (Fig. 2c) as a common phenomenon [10] is indicative of the material undergoing creep deformation. The increased time leads to a decrease in the softening coefficient, α, as clear in (Fig. 4b).

There is a clear temperature dependence, Fig. (1a-d), and time dependence, Fig. (2c) of alloy hardness. A tendency for Mg to segregate at the grain boundaries and sub-boundaries has been reported [4b]. This consists with the surface activity theory [29] which states that Mg atoms migrate to Al grain boundaries. As the amount of Mg is constant in the alloy, its contribution to hardness will depend mainly on the amount of free Mg available for hardening. Sargent and Ashby's model [30] based on dimensional analysis, was adopted here to analyze the obtained time dependent hardness data, Fig. (2c). Accordingly, the stress exponent, n, of 5.4 obtained for the binary alloy falls in the climb regime for which n is generally taken to be about, 5, [31]. The values of n in the range 6-7.8 may consist with dislocation glide as diffusion controlled process. For higher values of n up to 25.9 the probable mechanism is dislocation interaction [32].

Conclusion

1- Age hardening curves of Al-Mg alloy showed a leveling off and pronounced oscillations in the temperature range 443-503 K.
2- The alloy exhibit a typical dendritic structure. When increasing temperature, the dendritic structures become more obvious, and the dendrites are gradually refined.
3- The increased time leads to a decrease in the softening coefficient, α,
4- In general, increasing temperature, dwell time, applied load caused a decrease in hardness.
5- The values of n in the range 6-7.8 may consist with dislocation glide as diffusion controlled process. For higher values of n up to 25.9 the probable mechanism is dislocation interaction.

Acknowledgment

The authors are grateful to Prof. Dr. Asaad Mohamed Abdel Khalek, Physics Dept. of, Faculty of Education, Ain Shams Univ. for his help during the preparation of the paper.

References:

1. Mohamed A. M.A, Samuel F.H., Samuel A.M., Doty H.W.and Valtierra S.; *Metal.Mater. Trans*. A **39A**, 490 (2008).
2. Xu Sy and Long Sy; *LIFG. Mater. Sci. Forum*, **113**, 546 (2007).
3. Wen S. P., Xing Z. B. , Huang H. , Li B. L. , Wang W. and Nie Z. R. ; *Mater. Sci. Eng.*, A **516**, 42 (2009).
4. Mondolfo L.F.; Aluminium Alloys: Structure and properties, Butterworth & Co. (Publishers) ltd, (1976), The White Friars Press Ltd, London & Tonbridge. a) 377-380, b) 311-323.
5. Gaber A., Afify N., Abdel-Latief A.Y. and Mostafa M.S.; *Solid state Communications*, **86**, 10, 679 (1993).
6. Sundar R. S., Kutty T. R. G. and Sastry D. H.; *Intermetallics*, **8**, 427 (2000).
7. Sharma G., Ramanujan R. V., Kutty T. R. G. and Tiwari G. P.; *Mater. Sci. Eng*. A **278**, 106 (2000).
8. Petty E. r., Óneill H.; *Metallurgia*, **63**, 25 (1961).
9. Abd El-salam F., Wahab L. A., Nada R. H. and Zahran H. Y. ; *J. Mater. Sci*., **42**, 3661 (2007).
10. Batla Calleja F.J., Flores A., Ania F. and Basset D.C.; *J. Mater. Sci*., **35**, 1315 (2000).
11. Batla Calleja F. J.; *Trends Polym. Sci*., **66**, 17 (1985).
12. Cal X., Yang X. and Zhou P.; *J. Mater. Sci. Lett*. **16**, 741 (1997).
13. Manika I. and Manika J.; *Acta Materialia*, **54**, 2049 (2006).
14. Meng, X.Y., Northwood, D.O. and Smith, I. O.; *Metallography*, **19**, 285 (1986).
15. Rosenfeld A. M. and Timsit R. S.; *Phil. Mag*. B **49** (2), (1984).
16. Shin P. W. and Meshii M.; *J. Metals*, **15**, 80 (1963).
17. Kovács, I. and El-Sayed, H.; *Mater. Sci. Eng*. **20**, 123 (1975).
18. Lloyd D. J.; *Mater. Sci. Forum*, **519**, 55 (2006).
19. Sushanta K. P. and Jayaganthan R.; *Mater. Sci. Eng*., A **480**, 299 (2008).
20. Dragomir I. C., Gheorghe M., Thandhani N. and Snyder R. L.; *Mater. Sci. Eng*., A **402**, 158 (2005).

21. [21] Nakayama Y., Takaai T., Jin D. and Yamada Y.; *J. Jap Inst. Met*. **61**, 34 (1997).
22. [22] Nicolis G,Prigojin I, Self Organization in Nonequilibrium Systems, New York: Wiley; (1977).
23. Klose F. B., Hagemann F., Hähner P. and Neuhäuser H. ; *Mater. Sci. Eng*. A **387**, 93 (2004).
24. Lebyodkin M. A. and Estrin Y.; *Acta Materialia*, **53**, 3403 (2005).
25. Ait-Amokhtar H, Fressengeas C, Boudrahem; *Mater. Sci. Eng*. A **488**, 540 (2008).
26. Cormick P. G. Mc;Trans Indian. *Inst. Met*. **39**, 98 (1986).
27. Dong-Yeob P. and Marek N.; *Mater. Sci. Eng*. A **491**, 88 (2008).
28. Hassan S.B. and Aigbodion V.S.; *J.Alloys and Comp*., **486**, 309 (2009).
29. Semenchenko V. K.; Surface Phenomena in metals and alloys; London: Pergamon; 961.
30. Sargent P.M. and Ashby M.F.; *Mater. Sci. Tech*., **8**, 594 (1992).
31. Linga Murty K. and Ravi J.; *Wiratmo Nuc. Eng. Des*. **156**, 359 (1995).
32. Kutty T.R.G., Jarvis T. and Ganguly C.; *J. Nuc. Materials*, **246**, 189 (1997).